Analytica Chimica Acta 1131 (2020) 109–117

Contents lists available at ScienceDirect

Analytica Chimica Acta

journal homepage: www.elsevier.com/locate/aca

Polydopamine coated zirconium metal-organic frameworks-based immunochromatographic assay for highly sensitive detection of deoxynivalenol

Rui Li [1], Tong Bu [1], Yijian Zhao [1], Xinyu Sun , Qinzhi Wang , Yongming Tian , Feier Bai , Li Wang [*]

College of Food Science and Engineering, Northwest A&F University, Yangling, 712100, Shaanxi, China

HIGHLIGHTS

- A Zr-MOFs-polydopamine (ZrPA) based sensor was employed for deoxynivalenol detection.
- The ZrPA shares the merits of excellent water-stability and water-dispersibility.
- This assay has an 8-fold improved sensitivity than gold nanoparticles (GNPs)-sensor.
- The approach exhibited high selectivity and excellent food sample application ability.
- This work expands the application of MOFs as a novel label in immunoassays.

GRAPHICAL ABSTRACT

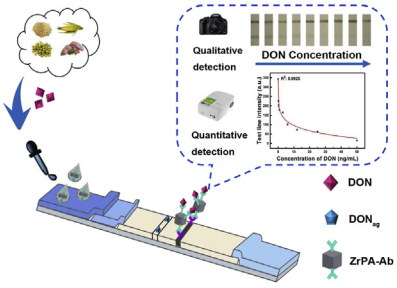

ARTICLE INFO

Article history:
Received 23 June 2020
Received in revised form
17 July 2020
Accepted 20 July 2020
Available online 31 July 2020

Keywords:
Immunochromatographic assays
Zirconium metal-organic frameworks
Deoxynivalenol
Novel probe

ABSTRACT

Conventional immunochromatographic assays (ICAs) based on gold nanoparticles (GNPs) suffer from the disadvantage of low sensitivity. In this work, a highly sensitive ICA based on polydopamine coated zirconium metal-organic frameworks labeled antibodies (ZrPA-Ab) as a novel probe was developed for visual determination of deoxynivalenol (DON). The ZrPA was synthesized via an oxidative self-polymerized assembly (OPMA) strategy using porphyrin functionalized zirconium metal-organic frameworks (Zr-MOFs, MOF-525) and polydopamine (PDA). The Abs could directly attach to the ZrPA surface owing to the large specific surface area, excellent water-stability and bio-compatibility of the ZrPA, on this basis, a sensitive, precise and reliable immunoassay method can be developed for rapid and selective detection of DON. Under optimized conditions, a non-linear calibration curve was obtained in the range of 0–50 ng/mL DON concentration with an IC_{50} of 1.22 ng/mL, and the visual detection limit was 0.18 ng/mL, which was about 8-times more sensitive than that of the conventional GNPs-based ICA. Finally, the proposed ZrPA-ICA was successfully applied for the detection of DON in pig hind legs meat, green bean, maize and millet samples, revealing the feasible and reliable application of this biosensor in different food matrices. Thus, this work broadens the possibilities for the use of MOFs as a novel labeling carrier in immunoassays.

* Corresponding author.
E-mail address: lwang@nwsuaf.edu.cn (L. Wang).
[1] These authors contributed equally to this work.

https://doi.org/10.1016/j.aca.2020.07.052
0003-2670/

1. Introduction

Deoxynivalenol (DON), a secondary metabolite generated by several Fusarium fungi species, is extensively exist in nature and generally contaminate many cereals such as corn, wheat, maize, rice and other grains [1,2]. However, the widespread contamination of DON in cereal products potentially causes harmful effects to animals and human, including diarrhea, vomiting, neurotoxicity and reproductive toxicity [3,4]. To ensure the human health, the European Union has set maximum residue level of DON (12 mg/kg) in maize by-products [5]. It is urgent to establish a reliable, rapid and efficient method for the DON determination in food stuffs.

Immunochromatographic assays (ICAs), also named as the lateral flow assay or test strip, is one of the most common point-of-need test analytical methods and has been used to detect DON [6–8]. Colloidal gold nanoparticles (GNPs) based ICAs are feasible but show relatively low sensitivity, which can't meet the requirements of ultrasensitive detection of analytes and has impeded their broad application, especially in the detection of trace analyte. It is reported that in terms of competitive ICAs, the sensitivity depends on the limited number of antibodies (Abs) and powerful carriers [9–11]. Very recently, several novel materials, such as Raman nanomaterials [12,13], quantum dots [14–16], fluorescent nanoprobes [17], silver nanoparticles [18,19], and other carriers rely on the use of non-traditional noble metal nanoparticles like non-spherical GNPs [20,21], have been employed as carriers for ICAs detection. Moreover, enzyme carriers that allow chemiluminescence detection have also been used [22,23]. The sensitivity of the ICAs have been highly improved by using those probes. However, these materials also suffer from the sophisticated binding process with Ab (organic cross-linking agents such as ethyl carbodiimide hydrochloride and N-hydroxysuccinimide (EDC/NHS) or glutaraldehyde are usually required to activate functional groups), which may result in the activity reduction or even denaturation of antibodies and thereby affecting the sensitivity [24]. Therefore, it is necessary to find suitable carriers to improve the sensitivity, which neither require redundant Abs nor complex synthesis or cross-linking steps.

Metal-organic frameworks (MOFs) are a kind of highly ordered crystalline materials composing of metal ion/cluster and organic linkers [25,26]. MOFs have acquired considerable application in heterogeneous catalysis, chemical sensing and biosensing owing to their remarkable properties [27,28]. Among these MOFs, zirconium-based MOFs (Zr-MOFs) possess excellent water-stability and water-dispersibility, which can be applied as a biological platform to detect various cancer markers or other analytes [29–31]. Furthermore, Zr-MOFs share high affinity property, which are easily to conjugate biomolecules, and have controlled particle sizes ranging from one hundred to several hundred nanometers [32,33]. These characteristics make them desirable carriers to construct ICAs. However, the exploration of the interaction between MOF and antibody is still at an early stage.

In this work, we developed a novel biosensing platform based on Zr-MOFs-polydopamine (ZrPA) with clearly black color and prominent affinity ability to Abs for ultrasensitive detection of DON. By using porphyrin functionalized Zr-MOFs (MOF-525) as a precursor, polydopamine (PDA) layer was coated on its surface via an oxidative self-polymerized assembly (OPMA) strategy to synthesize a highly water-stable and good bio-compatible ZrPA, which was then applied as a forceful carrier in ICAs to bind Abs easily and stably. The introduction of ZrPA-Ab probes avoided a series of troublesome Abs labeling steps and also the usage of complex cross-linking agents, providing an exceptional alternative candidate to conventional probes. Through a competitive immunoreaction, the ZrPA-Ab probes would competitively bind to DON in the solution and DON-antigen (DON_{ag}) on the T-line, showing a more distinct visible signal and an improved sensitivity (8 times than GNPs-based ICA). Combining these advantages, the ZrPA-ICA could observably upgrade the analytical performance for DON detection compared to the traditional GNPs-based ICA. Additionally, the proposed ZrPA-ICA was successfully applied in samples, containing pig hind legs meat, green bean, maize and millet, implying its great potential in the ultrasensitive on-site determination of analytes in food production.

2. Experimental

2.1. Reagents and materials

Meso-tetra (4-carboxyphenyl) porphine (H_4TCPP), zirconyl chloride octahydrate and dopamine hydrochloride ($ZrOCl_2 \cdot 8(H_2O)$), $HAuCl_4 \cdot 3H_2O$, trisodium citrate ($Na_3C_6H_5O_7 \cdot 2H_2O$), N, N-Dimethylformamide (DMF) and benzoic acid were obtained from Aladdin. (Shanghai, China). NaCl, $Na_2HPO_4 \cdot 2H_2O$, KCl, and KH_2PO_4 were purchased from Sinopharm Group (Beijing, China). Nitrocellulose (NC) high-flow membranes were received from Sartorius (Munich, Germany). Polyvinylchloride (PVC) backing cards were supplied by KeHua Bio-engineering Co., Ltd. (Shanghai, China), sample pads and absorbent pads were purchased from Shanghai Shiyibio Co., Ltd. (Shanghai, China). DON, patulin (PAT), aflatoxin B_1 (AFB_1), fumonisin (FB_1), zearalenone (ZEN), ochratoxin A (OTA) and ochratoxin B (OTB) and (Chemical structures were displayed in Fig. S1) were gained from feather flower biological science and Technology Co., Ltd. (Shanghai, China). Bovine serum albumin (BSA) was purchased from haosibiotech (Beijing, China). Anti-DON Abs and DON antigen (DON_{ag}, DON-BSA) were acquired from abcam trading Co., Ltd. (Shenzhen, China). Goat anti-mouse immunoglobulin (IgG) antibody was obtained from gilead sciences (Foster, CA, USA). Pig hind legs meat, green bean, maize and millet were acquired from a local supermarket (Yangling, China).

2.2. Instruments

Guillotine cutting machine and XYZ dispensing platform were purchased from Feng Hang Technology Co., Ltd. (Hangzhou, China). The centrifuge was provided by Tianmei Scientific Instrument Co., Ltd. (Shanghai, China). The strip results reader was acquired from Hemai Precision Instrument Co., Ltd. (Suzhou, China). Field emission scanning electron microscopy (SEM) and atomic force microscopy (AFM) were used for morphology characterization. Energy dispersive X-ray spectroscopy (EDX) was applied for elemental content. X-ray diffraction (XRD) was used to characterize the crystalline structure. The chemical states of the elements were examined by X-ray photoelectrons spectroscopy (XPS). The Fourier transform infrared spectroscopy (FT-IR) was measured by using Nicolet Nexus 470 (Bruker Corp, Germany). The zeta potentials were obtained from Zetasizer Nano-ZS instrument. The UV–visible (UV–vis) absorption spectrum results were tested with an PE lambda 750S (Shimadzu, Japan).

2.3. Preparation of MOF-525 and ZrPA

The MOF-525 was synthesized by a simple hydrothermal procedure [34]. Briefly, 2.7 g of carboxybenzene and 210 mg of $ZrOCl_2 \cdot 8(H_2O)$ were adding in 16 mL of DMF in a 40 mL screw-cap bottle to fully dissolve through sonication. The bottle was placed into the electric blast drying oven at 80 °C for reacting 2 h. After the

mixtures cooling to room temperature, 94 mg of H_4TCPP was dissolved to the above mixtures, and sonicated at room temperature for 20 min. Next, the purple solution was put in an oven with the temperature set at 80 °C for 24 h. The resulting product was obtained by centrifugation, then washed three times alternately with ethanol and DMF.

The ZrPA was prepared using an OPMA strategy [35]. Briefly, the 20 mg dried MOF-525 powder was added in a mixture of solution ethanol and water (35 mL, 3:4, v/v) under sonication for dispersion. Subsequently, 25 mg dopamine hydrochloride was added into the above solution under a vigorous stirring. Next, 25 mL of Tris-HCl buffer (10 mM, pH 8.8) was injected into the solution for 24 h in a dark place with a gentle stirring. Finally, the products were centrifuged (10 min, 20 °C, 10,380 *g*) and cleaned with ethanol and ultrapure water alternately for three times.

2.4. Conjugation of ZrPA-Ab probe

4 μg amount of anti-DON Abs solution (1 mg/mL) was added to 1 mL ZrPA solution (0.6 mg/mL). After the mixture incubated for 1 h at room temperature under gentle vortex stirring, 100 μL of BSA (10%, w/v) was added to react 1 h. The product was kept in 4 °C for another 2 h and then centrifuged (19,200 *g*, 15 °C, 30 min) to remove the unconjugated protein. The precipitate was resuspended in 100 μL ultrapure water and stored in 4 °C for the further experiments.

2.5. Construction of ICA strip

As depicted in Scheme 1, the ICA strip included five parts of NC high-flow membrane, sample pad, conjugate pad, absorbent pad and PVC card (used for fixing the mentioned four stuffs). The sample and conjugate pads were blocked by PBS buffer (10 mM aqueous solution containing 8.0 g NaCl, 2.9 g $Na_2HPO_4 \cdot 2H_2O$, 0.2 g KCl, 0.2 g KH_2PO_4 and 2% BSA), then dried overnight. The absorbent pad was utilized without any pretreatment. 1 mg/mL of DON_{ag} and 0.5 mg/mL of goat anti-mouse IgG were separately spread onto the NC high-flow membrane to form the T-line and C-line, at a spraying rate of 0.6 μL/cm and 1 μL/cm respectively. Afterward, the NC high-flow membrane was dried for 1 h at room temperature. NC membrane was first pasted on the PVC card. Subsequently, conjugate pad, sample pad and absorbent pad were assembled successively on a PVC card with about 1–2 mm overlapping. Finally, the equipped assay card was then cut into strips with 3 mm width and stored at desiccator.

2.6. Immunoassay detection process and performance assessment of ICA biosensors

Firstly, 2.5 μL of ZrPA-Ab probe was added into 100 μL of different concentrations of DON (0, 0.18, 0.37, 0.75, 3.0, 6.0, 12, 25 and 50 ng/mL, 10 mM PBS, not containing BSA), respectively. The sample pad was immerged into the above solution to allow all liquid can flow to the assay. After reacted for 10 min, the initial qualitative results were acquired by observing the black band with naked-eyes. The T-line intensity was read out by a strip reader to obtain the quantitative results.

The specificity of the ZrPA-ICA was verified by measuring DON (6.0 ng/mL) and other mycotoxins, which includes AFB_1, FB_1, ZEN, PAT, OTA and OTB (100 ng/mL).

2.7. Sample pretreatment

Green bean, maize, millet and pig hind legs were selected as practical samples to further evaluate the application value of the ZrPA-ICA. These samples were previously confirmed using high

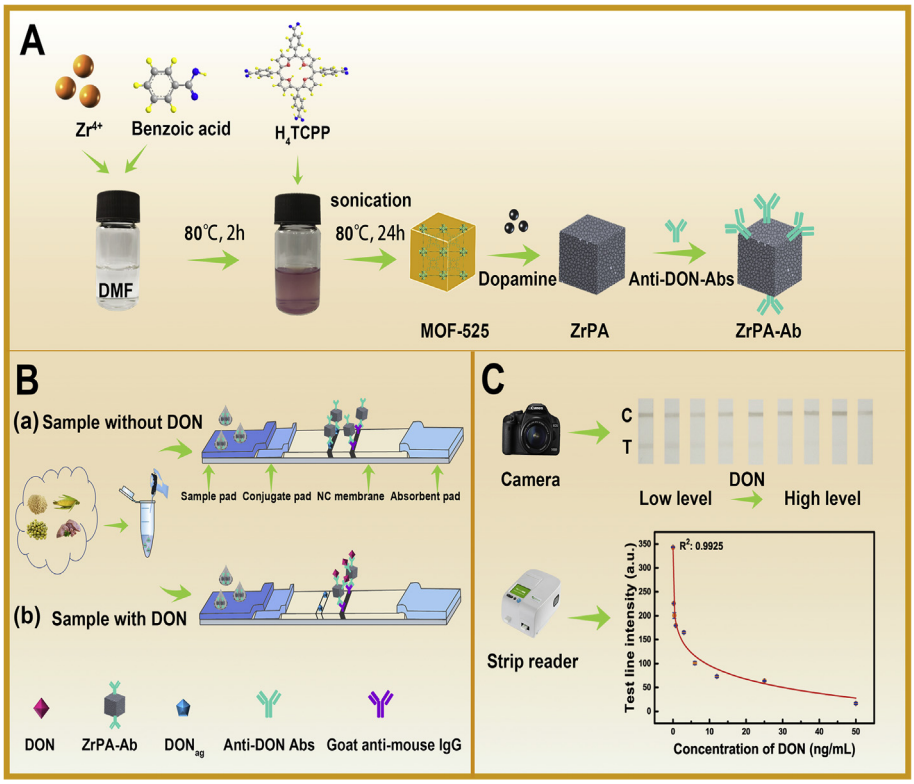

Scheme 1. (A) Schematic illustration of the synthesis steps of MOF-525, ZrPA and ZrPA-Ab. (B) Working principle of the ZrPA-ICA for detecting DON. (C) Interpretation of the assay results.

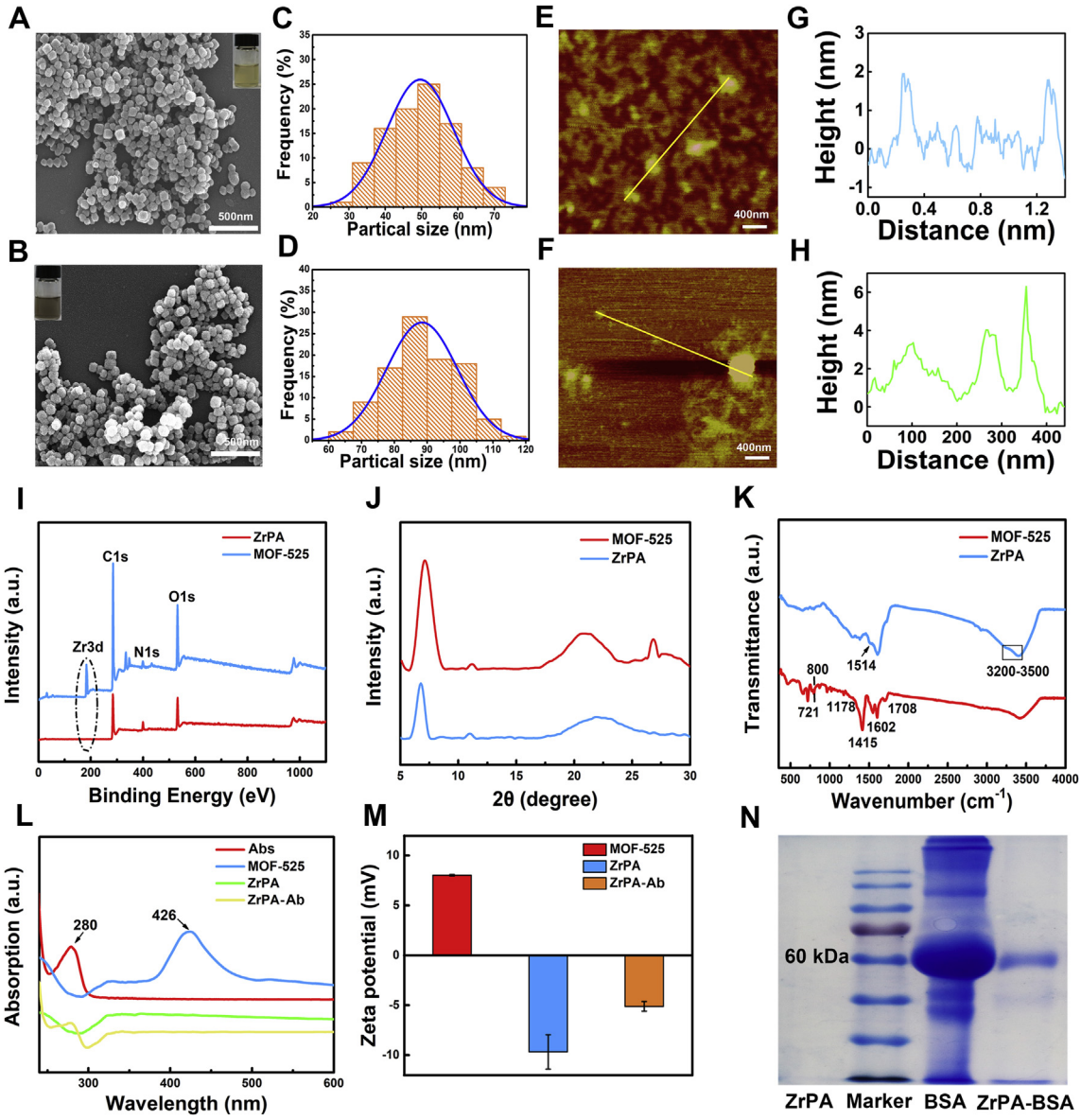

Fig. 1. SEM images and particle size of (A, C) MOF-525 and (B, D) ZrPA, respectively. AFM images and thickness distribution of (E, G) MOF-525 and (F, H) ZrPA, respectively. (I)–(K) XPS, XRD, and FT-IR spectra of MOF-525 and ZrPA, respectively. (L) UV–vis absorption spectra of Abs, ZrPA and ZrPA-Ab. (M) Zeta potential of MOF-525, ZrPA and ZrPA-Ab. (N) SDS-PAGE images of ZrPA, BSA and ZrPA-BSA, respectively.

performance liquid chromatography (HPLC) for nonexistence of DON before treatment, and the results were shown in Fig. S2. Those samples were pretreated according to the method performed in a previous study with some modification [36]. Briefly, 2 g of these dried foods were ground and extracted with methanol-water solution (6:4, 10 mL, v/v) for 15 min on a vortex mixer. After being centrifuged (5300 *g*, 10 min, 20 °C), the supernatant solution was spiked with DON at different concentration levels ranging from 1.8 to 500 ng/g. The resulting DON spiked samples were stored at 4 °C and further diluted 2-fold with PBS (10 mM, pH 7.0, not containing BSA) for ZrPA-ICA analysis.

3. Results and discussion

3.1. Preparation of ZrPA and principle of ZrPA-ICA biosensor

The synthesis steps of MOF-525, ZrPA and ZrPA-Ab were depicted in Scheme 1A. Firstly, MOF-525 with good water-stability was prepared. Subsequently, ZrPA was obtained by the OPMA strategy using MOF-525 as a precursor and PDA as a coating agent. Additionally, the Abs could easily bind to the ZrPA surface via a simple oscillation and incubation.

The ZrPA-ICA was based on competitive immunoassay principle (Scheme 1B). In the absence of the target DON, ZrPA-Ab probes would capture DON_{ag} to generate a black color on T-line, and then the extra probes keep moving forward and combine with the goat anti-mouse IgG on C-line, which also shows bright black band (as shown in Scheme 1B-a). In the presence of the target DON, the ZrPA-Ab probes competitively bind DON in the sample solution and DON_{ag} on the T-line. Thus, a weaker black band would be observed and the T-line intensity was inversely proportional to the DON concentration. When the DON concentration was high enough, no excess ZrPA-Ab probes were caught by the DON_{ag} and no visible black band on T-line would be observed (as shown in Scheme 1B-**b**). In addition, the strips result could be read by the naked-eye or photographed with camera for qualitative detection, and recorded

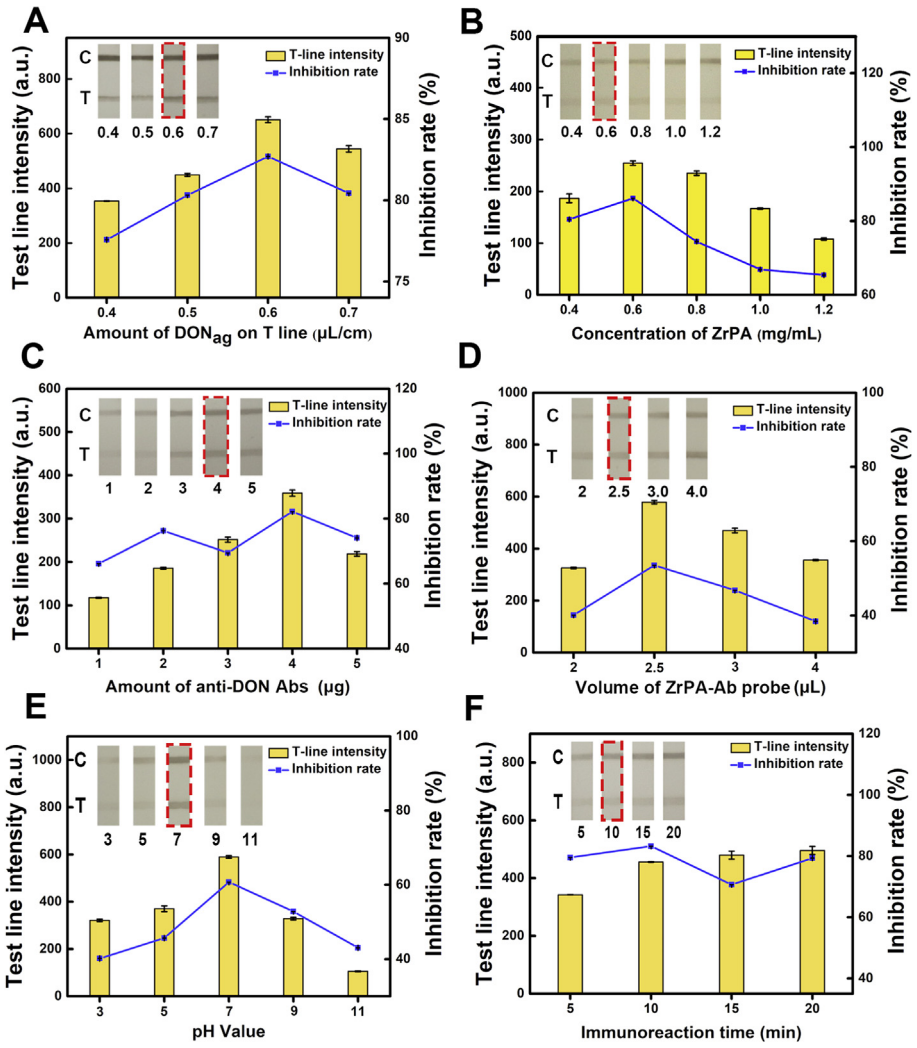

Fig. 2. The effects of (A) the amount of DON_{ag} on T-line, (B) the concentration of ZrPA, (C) the amount of anti-DON Abs, (D) the volume of the ZrPA-Ab probe, (E) pH value on the T-line signal, and (F) the immunoreaction time for detection of DON.

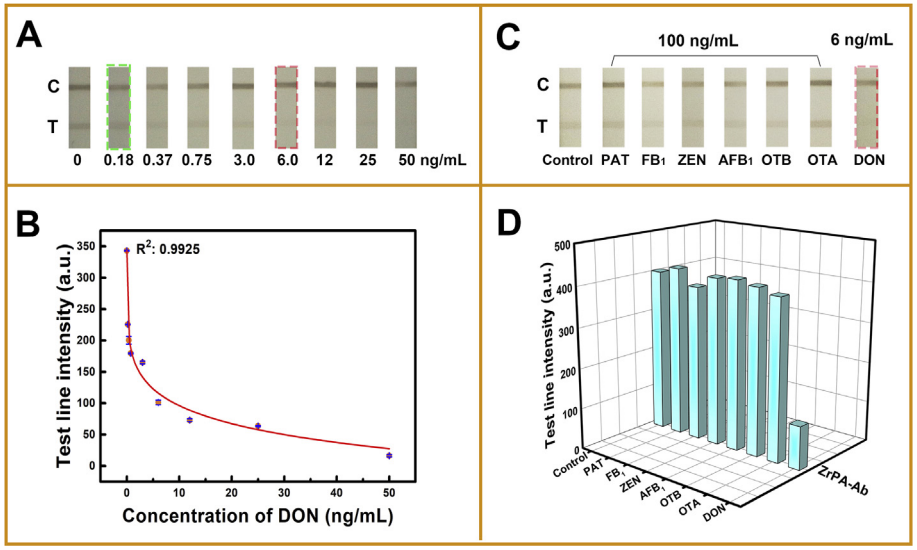

Fig. 3. (A) Sensitivity results of ZrPA-ICA for DON detection. (B) The variation rule in the 0–50 ng/mL range of DON using the ZrPA-ICA. (C) and (D) Specificity of the assay with other different interfering mycotoxins.

Table 1
Comparison of sensing performance for DON detection with other methods and ICAs based on different probes.

Methods	vLOD or LOD	Working range	Ref.
AgNPs-SERs[a]	100 nM	10^{-7}–10^{-2} mol/L	[1]
QDs dcFLISA[b]	12.2 μg/kg	50–200 μg/kg	[44]
QD@SiO_2ML[c]	35 ng/mL	55–420 ng/mL	[45]
Sas-TiO_2ECL[d]	16.7 ng/mL	0.00005–5 ng/mL	[46]
GNPs-ICA	2.5 ng/mL	2.5–100 ng/mL	[6]
GNPs-ICA	10 ng/mL	–	[47]
GNPs-LFA[e]	80 ng/mL	0–160 ng/mL	[8]
FGN-ICS[f]	5.0 ng/mL	0–20 ng/mL	[48]
QBs-LFA[g]	0.5 ng/mL	0–35 ng/mL	[49]
Eu@MNPs-ICA[h]	0.5 ng/mL	0.05–100 ng/mL	[50]
ZrPA-ICA	0.18 ng/mL	0.18–50 ng/mL	This work

[a] SERs, surface enhanced raman scattering.
[b] QDs dcFLISA, quantum dot direct competitive fluorescent-labeled immunosorbent assay.
[c] QD@SiO_2 ML, silica coated quantum dots multiplex luminescent.
[d] Sas-TiO_2 ECL, surfactant-assisted synthesis of TiO_2mesocrystals electrochemiluminescence.
[e] LFA, lateral flow immunoassay.
[f] FGN-ICS, flower-like gold nanoparticles-based immunochromatographic test strip.
[g] QBs, quantum dot microbeads.
[h] Eu@MNPs, europiumchelates and magnetic nanoparticles.

by strip reader for quantitative determination (Scheme 1C).

3.2. Characterization of MOF-525, ZrPA composites and ZrPA-Ab probe

As shown in Fig. 1A, the prepared MOF-525 was uniformly cubes and its average diameter was approximately at 49.65 nm. After reaction with a certain amount of dopamine, the color of the suspension changed from yellow (Fig. 1A, right inset) to black (Fig. 1B, left inset). In addition, the ZrPA maintained the shape of cube with an average particle size of about 88.44 nm. The EDX proved that the main elements of the ZrPA were C and Zr (Fig. S3). Besides, the AFM images (Fig. 1E–H) further confirmed that the average thicknesses of MOF-525 and ZrPA were approximately 1 nm and 4 nm, respectively, indicating that the thickness of ZrPA was increased after PDA-coating process. The XPS results (Fig. 1I) showed the peaks appeared at 182.9, 284.9, 399.9 and 531.9 eV, which attributed to Zr 3d, C 1s, N 1s and O 1s in the MOF-525 [37]. However, the peak at 182.9 eV, assigned to the Zr 3d in MOF-525, was absent in the spectrum of ZrPA, which further proved the successful preparation of ZrPA. The high-resolution spectrum of C 1 s, N 1s and O 1s were displayed in Fig. S4.

Diffraction peaks of MOF-525 located at $2\theta = 6.8^{\circ}$ and 10.9°; these peaks were consistent with the previously reported literature [38]. Compared with MOF-525, the main diffraction peak of ZrPA composites were the same as that of MOF-525, while the intensity was reduced, which proved the successful combination of MOF-525 and PDA (Fig. 1J). Furthermore, the FT-IR spectra showed that MOF-525 had the characteristic bands (1708, 1602, 1415, 1178, 869, 800, 775, and 721 cm^{-1}) that were correspond to the previously report [39]. Besides, three peaks were observed at 3200–3500 and 1514 cm^{-1} in ZrPA, which assigned to the stretching vibrations of O–H/N–H and ring vibration of indole of PDA, respectively (Fig. 1K). In the UV–vis spectra (Fig. 1L), the pure MOF-525 solution exhibited an absorption peak at 426 nm (red line) corresponding to the porphyrin family [40]. In contrast, the ZrPA had no absorption peak after the introduction of PDA, confirming that the PDA was covered on the surface of MOF-525 [35]. All the above results proved that ZrPA was successfully synthesized.

To further confirm the formation of the ZrPA-Ab probe, UV–vis spectra, Zeta potential and sodium dodecyl sulfate-polyacrylamide gel electrophoresis (SDS-PAGE) were investigated. In UV–vis spectra (Fig. 1L), after the addition of Abs, a new peak appeared at 280 nm (yellow one), which indirectly confirm that Abs had successfully connected to the ZrPA. Notably, in Fig. 1M, a clear change from −9.67 to −5.11 mV in the Zeta potential of ZrPA was observed after the addition of Abs. Interestingly, we found that the molecular weight of this probe remained at ~60 kDa after the binding with BSA, while the pure ZrPA did not show any bands (Fig. 1N). Based on the above verification, it can be concluded that protein was successfully immobilized on the surface of ZrPA.

3.3. Optimization of the experimental parameters

To obtain the best sensing performance of this ZrPA-ICA biosensor, the amount of DON_{ag} on T-line, the ZrPA concentration, amount of the anti-DON Abs, the amount of the ZrPA-Ab probe, pH and immunoreaction time were optimized. T-line with the strongest intensity as well as the highest inhibition rate was chosen as an optimal condition. In Fig. 2A, the intensity of the T-line was enhanced with the increasing of DON_{ag} on T line. Additionally, the inhibition rate was maximized at 0.6 μL/cm. Therefore, 0.6 μL/cm was chosen for further study. As displayed in Fig. 2B, the intensities of the two lines were gradually heightened with the increase of the ZrPA concentration, and the inhibition rate decreased from 80 to 65.37% as the concentration of ZrPA increased to 0.6 mg/mL. Thereby, 0.6 mg/mL was considered as the optimal ZrPA concentration. In test strip analysis, especially for small molecule sensing, the amount of Abs possesses a profound influence on the detection sensitivity. So, 1 mL of ZrPA (0.6 mg/mL) was mixed with 1 mg/mL of anti-DON Abs at various amounts (1–5 μg) to prepare ZrPA-Ab probe. The color of the T-line deepened gradually with the increasing of the amount of Abs, and highest inhibition rate (82.16%) was obtained at 4 μg (Fig. 2C). Thus, 4 μg Abs was chosen. Most importantly, the amount of antibody used was less than that of GNPs (5 μg, Fig. S5, and the condition optimization of GNPs-ICA was also shown in Supporting Information). Subsequently, in Fig. 2D, it can be observed that when probe volume was 2.5 μL, the colors of the two lines were closest and the inhibition rate was the highest. Therefore, 2.5 μL of the probe was selected for the further study. Additionally, Fig. 2E showed various responses resulting from various pH values (pH 3, 5, 7, 9 and 11). The brightest color on T-line was obtained when pH increased to 7. Therefore, pH = 7 was chosen for the next experiments. As displayed in Fig. 2F, the immune-reaction time of assays was optimized (5, 10, 15 and 20 min), the highest T-line intensity value was emerged at 10 min. Hence, the optimal immune-reaction time used for this biosensor was 10 min.

3.4. Analytical performance

Under optimal conditions, the ZrPA-ICA sensitivity for DON determination was investigated by testing various concentrations of standard DON solutions. The visual limits of detection (vLOD) was defined as the minimum DON concentration which produces observable weaker color on T-line compared with the control strip. The minimum detected DON concentration consistent to the test strip with the color completely disappeared on T-line was selected as the cut-off value. As shown in Fig. 3A, when the concentration of DON attained to 0.18 ng/mL, the T-line intensity was nearly weaker compared to the control strip and the T-line completely vanished at 6 ng/mL. Thus, the vLOD and cut-off value of the ZrPA-ICA for DON determination were 0.18 and 6 ng/mL, respectively. Furthermore, a typical calibration curve obtained from the ZrPA-ICA by using the following four-parameter sigmoidal function, with an IC_{50} of

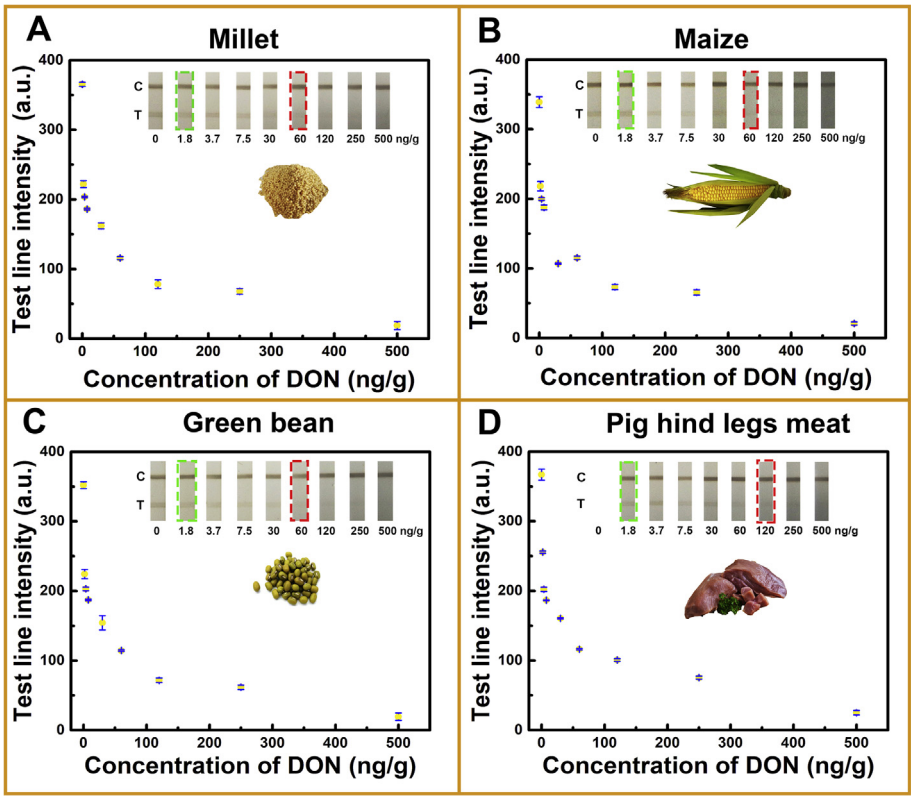

Fig. 4. Practicability test of the ZrPA-ICA for food samples detection. A-D represent millet, maize green bean and pig hind legs meat, respectively. (For interpretation of the references to color in this figure legend, the reader is referred to the Web version of this article.)

1.22 ng/mL (Fig. 3B).

$$y = \frac{783.0512}{1 + (\frac{x}{263.5136})^{0.2366}} - 439.9286 \quad (1)$$

However, the vLOD and cut-off value for the GNPs-ICA were around at 1.5 ng/mL and 50 ng/mL, respectively (Fig. S6A). So, it was at least 8-fold enhancement of the proposed ICA by applying ZrPA as the carriers compared to the traditional GNPs-ICA. In this work, we conclude that there are two reasons for the increased sensitivity. On the one hand, under the same experimental conditions, the black color of ZrPA that has a lower brightness on the NC membrane at 0 and 0.75 ng/mL DON concentration, respectively, in comparison to the red color of GNPs (Fig. S7). On the other hand, the sensitivity depends on the amount of antibody employed, decreasing of Ab: label molar ratio also could improve sensitivity [11,41–43]. In our experiment, the amount of antibody was 4 μg in ZrPA-ICA, instead of 5 μg for GNPs-ICA. Therefore, the sensitivity was highly improved by using ZrPA-ICA than that of GNPs-ICA. Additionally, compared with other methods (Table 1), the vLOD of ZrPA-ICA was lower than most literatures.

Specificity is a key parameter to investigate the performance of this biosensor. The specificity of the ZrPA-ICA was validated by several mycotoxins (PAT, FB_1, ZEN, AFB_1, OTA and OTB, 100 ng/mL) and DON (6 ng/mL). The results were present in Fig. 3C, the black color band on the T-line eliminated completely when adding only 6 ng/mL of DON. However, the T-line intensity for the other mycotoxins was the same as the control strip. The results of GNPs-ICA

Table 2
Recoveries of DON spiked in millet, maize, green bean and pig hind legs meat samples (n = 3).

Real samples	Added (ng/g)	Founded (ng/g)	Recovery (%)	RSD (%, n = 3)
Millet	3.7	4.1 ± 0.017	111.1	4.1
	7.5	7.6 ± 0.031	101.2	4.1
	60	60.4 ± 0.346	100.7	5.7
Maize	3.7	4.3 ± 0.005	115.4	1.1
	7.5	7.4 ± 0.038	100.6	5.1
	60	59.0 ± 0.345	98.4	5.8
Green bean	3.7	4.0 ± 0.024	107.1	6.2
	7.5	7.3 ± 0.025	97.8	3.5
	60	60.5 ± 0.251	100.8	4.1
Pig hind legs meat	3.7	4.1 ± 0.012	109.5	3.0
	7.5	7.5 ± 0.011	99.7	1.5
	60	59.7 ± 0.167	99.4	2.8

were consistent with the above method (Fig. S6B). The T-lines intensities were tested by recording the average numerical values of the black bands on the T areas (n = 3) (Fig. 3D). Therefore, the results show that the developed ICA biosensor possessed a prominent specificity for DON determination.

3.5. Practical application in real samples

In order to evaluate the potential practical application of the ZrPA-ICA in real samples, a variety of DON concentrations at 0, 1.8, 3.7, 7.5, 30, 60, 120, 250, 500 ng/g were added into millet, maize, green bean and pig hind legs meat for the spiked experiments. As depicted in Fig. 4, the vLODs of DON were about 1.8 ng/g in millet, maize, green bean and pig hind legs meat, and the cut-off values of DON were around at 60, 60, 60 and 120 ng/mL, respectively. The vLODs of GNPs-ICA were around at 15 ng/g in millet, maize, green bean and pig hind legs, while the cut-off results were 500, 500, 500 and 1000 ng/g, respectively (Fig. S8). The degraded performance in pig hind legs meat may be resulted from some interferents, such as a certain amount of fat or other salt ions included in supernatant solutions. Furthermore, the recoveries of these spiked samples were ranged from 97.8% to 109.5% with relative standard deviation (RSD) levels below than 7% (Table 2). These results demonstrated that the proposed ZrPA-ICA had the practicability for DON determination in practical samples.

4. Conclusion

In summary, a novel and feasible ICA biosensor was fabricated using ZrPA-Ab as a probe for ultrasensitive and specific DON detection. The ZrPA was successfully synthesized via a simple OPMA strategy. Thanks to the excellent water-stability, large specific surface area and bio-compatibility properties of the ZrPA, fewer Abs could be connected on the surface of carriers through an easy and facile mixing process, overcoming the drawback of using complex cross-linking agents. This immune sensing platform showed an improved performance to DON with a vLOD as low as 0.18 ng/mL, which was superior to traditional GNPs-based ICA and previous reports. Most importantly, the ZrPA-ICA was successfully applied to pig hind legs meat, green bean, maize and millet for DON determination. By introducing MOFs materials to improve the ICAs performance, our work provides a basis for immunoassays to select other alternative MOFs materials as carriers.

CRediT authorship contribution statement

Rui Li: Conceptualization, Methodology, Formal analysis, Writing - original draft. **Tong Bu:** Conceptualization, Methodology, Formal analysis, Writing - original draft. **Yijian Zhao:** Validation, Visualization. **Xinyu Sun:** Validation, Visualization. **Qinzhi Wang:** Validation, Visualization. **Yongming Tian:** Validation, Visualization. **Feier Bai:** Validation, Visualization. **Li Wang:** Conceptualization, Writing - review & editing, Supervision, Project administration.

Declaration of competing interest

The authors declare that they have no known competing financial interests or personal relationships that could have appeared to influence the work reported in this paper.

Acknowledgements

This work was supported by Talented Program (A279021724) and the Fundamental Research Funds for the Northwest A&F University (Nos. Z111021601).

Appendix A. Supplementary data

Supplementary data to this article can be found online at https://doi.org/10.1016/j.aca.2020.07.052.

References

[1] J. Yuan, C. Sun, X. Guo, T. Yang, H. Wang, S. Fu, C. Li, H. Yang, A rapid Raman detection of deoxynivalenol in agricultural products, Food Chem. 221 (2017) 797–802, https://doi.org/10.1016/j.foodchem.2016.11.101.
[2] A. Infantino, G. Aureli, C. Costa, C. Taiti, F. Antonucci, P. Menesatti, F. Pallottino, S. De Felice, M.G. D'Egidio, S. Mancuso, Potential application of PTR-TOFMS for the detection of deoxynivalenol (DON) in durum wheat, Food Contr. 57 (2015) 96–104, https://doi.org/10.1016/j.foodcont.2015.03.047.
[3] L.B. Bullerman, A. Bianchini, Stability of mycotoxins during food processing, Int. J. Food Microbiol. 119 (2007) 140–146, https://doi.org/10.1016/j.ijfoodmicro.2007.07.035.
[4] C. Zhu, G. Zhang, Y. Huang, S. Yang, S. Ren, Z. Gao, A. Chen, Dual-competitive lateral flow aptasensor for detection of aflatoxin B1 in food and feedstuffs, J. Hazard Mater. 344 (2018) 249–257, https://doi.org/10.1016/j.jhazmat.2017.10.026.
[5] European Commission, Commission Recommendation of 17 August 2006 on the presence of deoxynivalenol, zearalenone, ochratoxin A, T-2 and HT-2 and fumonisins inproducts intended for animal feeding, Off. J. Eur. Union L299 (2006) 7–9. https://eur-lex.europa.eu/legal-content/EN/TXT/PDF/?uri=CELEX:32006H0576&from=DE.
[6] D. Kong, X. Wu, Y. Li, L. Liu, S. Song, Q. Zheng, H. Kuang, C. Xu, Ultrasensitive and eco-friendly immunoassays based monoclonal antibody for detection of deoxynivalenol in cereal and feed samples, Food Chem. 270 (2019) 130–137, https://doi.org/10.1016/j.foodchem.2018.07.075.
[7] Z.B. Huang, Y. Xu, L.S. Li, Y.P. Li, H. Zhang, Q.H. He, Development of an immunochromatographic strip test for the rapid simultaneous detection of deoxynivalenol and zearalenone in wheat and maize, Food Contr. 28 (2012) 7–12, https://doi.org/10.1016/j.foodcont.2012.04.035.
[8] Q. Yu, H. Li, C. Li, S. Zhang, J. Shen, Z. Wang, Gold nanoparticles-based lateral flow immunoassay with silver staining for simultaneous detection of fumonisin B1 and deoxynivalenol, Food Contr. 54 (2015) 347–352, https://doi.org/10.1016/j.foodcont.2015.02.019.
[9] B. Zhao, Q. Huang, L. Dou, T. Bu, K. Chen, Q. Yang, L. Yan, J. Wang, D. Zhang, Prussian blue nanoparticles based lateral flow assay for high sensitive determination of clenbuterol, Sensor. Actuator. B Chem. 275 (2018) 223–229, https://doi.org/10.1016/j.snb.2018.08.029.
[10] T. Bu, M. Zhang, X. Sun, Y. Tian, F. Bai, P. Jia, Y. Bai, T. Zhe, L. Wang, Gold nanoparticles-functionalized microorganisms assisted construction of immunobiosensor for sensitive detection of ochratoxin A in food samples, Sensor. Actuator. B Chem. 299 (2019) 126969, https://doi.org/10.1016/j.snb.2019.126969.
[11] F. Di Nardo, S. Cavalera, C. Baggiani, C. Giovannoli, L. Anfossi, Direct vs mediated coupling of antibodies to gold nanoparticles: the case of salivary cortisol detection by lateral flow immunoassay, ACS Appl. Mater. Interfaces 11 (2019) 32758–32768, https://doi.org/10.1021/acsami.9b11559.
[12] J. Hwang, S. Lee, J. Choo, Application of a SERS-based lateral flow immunoassay strip for the rapid and sensitive detection of staphylococcal enterotoxin B, Nanoscale 8 (2016) 11418–11425, https://doi.org/10.1039/c5nr07243c.
[13] D. Deng, H. Yang, C. Liu, K. Zhao, J. Li, A. Deng, Ultrasensitive detection of diclofenac in water samples by a novel surface-enhanced Raman scattering (SERS)-based immunochromatographic assay using AgMBA@SiO2-Ab as immunoprobe, Sensor. Actuator. B Chem. 283 (2019) 563–570, https://doi.org/10.1016/j.snb.2018.12.076.
[14] F. Di Nardo, L. Anfossi, C. Giovannoli, C. Passini, V.V. Goftman, I.Y. Goryacheva, C. Baggiani, A fluorescent immunochromatographic strip test using Quantum Dots for fumonisins detection, Talanta 150 (2016) 463–468, https://doi.org/10.1016/j.talanta.2015.12.072.
[15] Y. Wang, Z. Li, H. Lin, P.N. Siddanakoppalu, J. Zhou, G. Chen, Z. Yu, Quantum-dot-based lateral flow immunoassay for the rapid detection of crustacean major allergen tropomyosin, Food Contr. 106 (2019) 106714, https://doi.org/10.1016/j.foodcont.2019.106714.
[16] C.C. Fang, C.C. Chou, Y.Q. Yang, T. Wei-Kai, Y.T. Wang, Y.H. Chan, Multiplexed detection of tumor markers with multicolor polymer dot-based immunochromatography test strip, Anal. Chem. 90 (2018) 2134–2140, https://doi.org/10.1021/acs.analchem.7b04411.
[17] G. Liang, Y. Shao, H. Duan, W. Ma, Y. Leng, H. Xiaolin, X. Yonghua, Magnetic quantum dot nanobead-based fluorescent immunochromatographic assay for the highly sensitive detection of aflatoxin B1 in dark soy sauce, Anal. Chem. 91 (2019) 4727–4734.
[18] L. Anfossi, F. Di Nardo, A. Russo, S. Cavalera, C. Giovannoli, G. Spano, S. Baumgartner, K. Lauter, C. Baggiani, Silver and gold nanoparticles as multichromatic lateral flow assay probes for the detection of food allergens, Anal. Bioanal. Chem. 411 (2019) 1905–1913, https://doi.org/10.1007/s00216-018-1451-6.
[19] K.H. Wu, W.C. Huang, S.C. Chang, C.H. Kao, R.H. Shyu, Colloidal silver-based lateral flow immunoassay for rapid detection of melamine in milk and animal feed, Mater. Chem. Phys. 231 (2019) 121–130, https://doi.org/10.1016/

j.matchemphys.2019.04.035.
[20] Y. Ji, M. Ren, Y. Li, Z. Huang, M. Shu, H. Yang, Y. Xiong, Y. Xu, Detection of aflatoxin B1 with immunochromatographic test strips: enhanced signal sensitivity using gold nanoflowers, Talanta 142 (2015) 206–212, https://doi.org/10.1016/j.talanta.2015.04.048.
[21] F. Di Nardo, E. Alladio, C. Baggiani, S. Cavalera, C. Giovannoli, G. Spano, L. Anfossi, Colour-encoded lateral flow immunoassay for the simultaneous detection of aflatoxin B1 and type-B fumonisins in a single Test line, Talanta 192 (2019) 288–294, https://doi.org/10.1016/j.talanta.2018.09.037.
[22] M. Zangheri, M. Mirasoli, M. Guardigli, F. Di, L. Anfossi, C. Baggiani, P. Simoni, M. Benassai, A. Roda, Biosensors and Bioelectronics Chemiluminescence-based biosensor for monitoring astronauts ' health status during space missions : results from the International Space Station, Biosens. Bioelectron. 129 (2019) 260–268, https://doi.org/10.1016/j.bios.2018.09.059.
[23] M. Zangheri, F. Di Nardo, M. Mirasoli, L. Anfossi, A. Nascetti, D. Caputo, G. De Cesare, M. Guardigli, C. Baggiani, A. Roda, Chemiluminescence lateral flow immunoassay cartridge with integrated amorphous silicon photosensors array for human serum albumin detection in urine samples, Anal. Bioanal. Chem. 408 (2016) 8869–8879, https://doi.org/10.1007/s00216-016-9991-0.
[24] S. Liu, L. Dou, X. Yao, W. Zhang, B. Zhao, Z. Wang, Y. Ji, J. Sun, B. Xu, D. Zhang, J. Wang, Polydopamine nanospheres as high-affinity signal tag towards lateral flow immunoassay for sensitive furazolidone detection, Food Chem. 315 (2020) 126310, https://doi.org/10.1016/j.foodchem.2020.126310.
[25] H.S. Wang, Metal–organic frameworks for biosensing and bioimaging applications, Coord. Chem. Rev. 349 (2017) 139–155, https://doi.org/10.1016/j.ccr.2017.08.015.
[26] P. Kumar, A. Deep, K.H. Kim, Metal organic frameworks for sensing applications, TrAC Trends Anal. Chem. (Reference Ed.) 73 (2015) 39–53, https://doi.org/10.1016/j.trac.2015.04.009.
[27] K.Y. Cho, J.Y. Seo, H.J. Kim, S.J. Pai, X.H. Do, H.G. Yoon, S.S. Hwang, S.S. Han, K.Y. Baek, Facile control of defect site density and particle size of UiO-66 for enhanced hydrolysis rates: insights into feasibility of Zr(IV)-based metal-organic framework (MOF) catalysts, Appl. Catal. B Environ. 245 (2019) 635–647, https://doi.org/10.1016/j.apcatb.2019.01.033.
[28] G.Y. Zhang, Y.H. Zhuang, D. Shan, G.F. Su, S. Cosnier, X.J. Zhang, Zirconium-based porphyrinic metal-organic framework (PCN-222): enhanced photoelectrochemical response and its application for label-free phosphoprotein detection, Anal. Chem. 88 (2016) 11207–11212, https://doi.org/10.1021/acs.analchem.6b03484.
[29] Z. Jia, Y. Ma, L. Yang, C. Guo, N. Zhou, M. Wang, L. He, Z. Zhang, NiCo 2 O 4 spinel embedded with carbon nanotubes derived from bimetallic NiCo metal-organic framework for the ultrasensitive detection of human immune deficiency virus-1 gene, Biosens. Bioelectron. 133 (2019) 55–63, https://doi.org/10.1016/j.bios.2019.03.030.
[30] C. Guo, F. Su, Y. Song, B. Hu, M. Wang, L. He, D. Peng, Z. Zhang, Aptamer-templated silver nanoclusters embedded in zirconium metal-organic framework for bifunctional electrochemical and SPR aptasensors toward carcinoembryonic antigen, ACS Appl. Mater. Interfaces 9 (2017) 41188–41199, https://doi.org/10.1021/acsami.7b14952.
[31] N. Zhou, F. Su, C. Guo, L. He, Z. Jia, M. Wang, Q. Jia, Z. Zhang, S. Lu, Two-dimensional oriented growth of Zn-MOF-on-Zr-MOF architecture: a highly sensitive and selective platform for detecting cancer markers, Biosens. Bioelectron. 123 (2019) 51–58, https://doi.org/10.1016/j.bios.2018.09.079.
[32] J.A. Harvey, C.J. Pearce, M.G. Hall, E.J. Bruni, J.B. Decoste, D.F. Sava Gallis, Insights into the solvent-Assisted degradation of organophosphorus compounds by a Zr-based metal-organic framework, Dalton Trans. 48 (2019) 16153–16157, https://doi.org/10.1039/c9dt03710a.
[33] F. Xiao, X. Hu, Y. Chen, Y. Zhang, Porous Zr-based metal-organic frameworks (Zr-MOFs)-Incorporated thin-film nanocomposite membrane toward enhanced desalination performance, ACS Appl. Mater. Interfaces (2019), https://doi.org/10.1021/acsami.9b17212.
[34] T.Y. Huang, C.W. Kung, Y. Te Liao, S.Y. Kao, M. Cheng, T.H. Chang, J. Henzie, H.R. Alamri, Z.A. Alothman, Y. Yamauchi, K.C. Ho, K.C.W. Wu, Enhanced charge collection in MOF-525–PEDOT nanotube composites enable highly sensitive biosensing, Adv. Sci. 4 (2017) 1–8, https://doi.org/10.1002/advs.201700261.
[35] R. Ren, G. Cai, Z. Yu, Y. Zeng, D. Tang, Metal-polydopamine framework: an innovative signal-generation tag for colorimetric immunoassay, Anal. Chem. 90 (2018) 11099–11105, https://doi.org/10.1021/acs.analchem.8b03538.
[36] Y. Shao, H. Duan, L. Guo, Y. Leng, W. Lai, Y. Xiong, Quantum dot nanobead-based multiplexed immunochromatographic assay for simultaneous detection of aflatoxin B1 and zearalenone, Anal. Chim. Acta 1025 (2018) 163–171, https://doi.org/10.1016/j.aca.2018.03.041.
[37] M. Cao, X. Yin, X. Bo, L. Guo, High-performance electrocatalyst based on metal-organic framework/macroporous carbon composite for efficient detection of luteolin, J. Electroanal. Chem. 824 (2018) 153–160, https://doi.org/10.1016/j.jelechem.2018.07.049.
[38] C.W. Kung, T.H. Chang, L.Y. Chou, J.T. Hupp, O.K. Farha, K.C. Ho, Post metalation of solvothermally grown electroactive porphyrin metal-organic framework thin films, Chem. Commun. 51 (2015) 2414–2417, https://doi.org/10.1039/c4cc09272d.
[39] D. Feng, Z.Y. Gu, J.R. Li, H.L. Jiang, Z. Wei, H.C. Zhou, Zirconium-metalloporphyrin PCN-222: mesoporous metal-organic frameworks with ultrahigh stability as biomimetic catalysts, Angew. Chem. Int. Ed. 51 (2012) 10307–10310, https://doi.org/10.1002/anie.201204475.
[40] T.Y. Chen, Y.J. Huang, C.T. Li, C.W. Kung, R. Vittal, K.C. Ho, Metal-organic framework/sulfonated polythiophene on carbon cloth as a flexible counter electrode for dye-sensitized solar cells, Nanomater. Energy 32 (2017) 19–27, https://doi.org/10.1016/j.nanoen.2016.12.019.
[41] L. Anfossi, F. Di Nardo, C. Giovannoli, C. Passini, C. Baggiani, Increased sensitivity of lateral flow immunoassay for ochratoxin A through silver enhancement, Anal. Bioanal. Chem. 405 (2013) 9859–9867, https://doi.org/10.1007/s00216-013-7428-6.
[42] E.A. Zvereva, N.A. Byzova, P.G. Sveshnikov, A.V. Zherdev, B.B. Dzantiev, Cut-off on demand: adjustment of the threshold level of an immunochromatographic assay for chloramphenicol, Anal. Methods. 7 (2015) 6378–6384, https://doi.org/10.1039/c5ay00835b.
[43] L. Anfossi, C. Baggiani, C. Giovannoli, F. Biagioli, G. D'Arco, G. Giraudi, Optimization of a lateral flow immunoassay for the ultrasensitive detection of aflatoxin M1 in milk, Anal. Chim. Acta 772 (2013) 75–80, https://doi.org/10.1016/j.aca.2013.02.020.
[44] X. Zhang, X. Yu, J. Wang, Q. Wang, H. Meng, Z. Wang, One-step core/multishell quantum dots-based fluoroimmunoassay for screening of deoxynivalenol in maize, Food Anal. Methods. 11 (2018) 2569–2578, https://doi.org/10.1007/s12161-018-1198-x.
[45] N. Beloglazova, P. Lenain, M. Tessier, I. Goryacheva, Z. Hens, S. De Saeger, Bioimprinting for multiplex luminescent detection of deoxynivalenol and zearalenone, Talanta 192 (2019) 169–174, https://doi.org/10.1016/j.talanta.2018.09.042.
[46] H. Zheng, Y. Ke, H. Yi, H. Dai, D. Fang, Y. Lin, Z. Hong, X. Li, A bifunctional reagent regulated ratiometric electrochemiluminescence biosensor constructed on surfactant-assisted synthesis of TiO2 mesocrystals for the sensing of deoxynivalenol, Talanta 196 (2019) 600–607, https://doi.org/10.1016/j.talanta.2018.12.077.
[47] S. Yu, L. He, F. Yu, L. Liu, C. Qu, L. Qu, J. Liu, Y. Wu, Y. Wu, A lateral flow assay for simultaneous detection of Deoxynivalenol, Fumonisin B 1 and Aflatoxin B 1, Toxicon 156 (2018) 23–27, https://doi.org/10.1016/j.toxicon.2018.10.305.
[48] X. Huang, T. Huang, X. Li, Z. Huang, Flower-like gold nanoparticles-based immunochromatographic test strip for rapid simultaneous detection of fumonisin B1 and deoxynivalenol in Chinese traditional medicine, J. Pharmaceut. Biomed. Anal. 177 (2020) 112895, https://doi.org/10.1016/j.jpba.2019.112895.
[49] R. Li, C. Meng, Y. Wen, W. Fu, P. He, Fluorometric lateral flow immunoassay for simultaneous determination of three mycotoxins (aflatoxin B1, zearalenone and deoxynivalenol) using quantum dot microbeads, Microchim. Acta. 186 (2019), https://doi.org/10.1007/s00604-019-3879-6.
[50] B. Zhou, X. Yuan, Y. Hu, J. Fan, W. Yang, M. Guo, Y. Zhang, W. Li, J. Zhang, Detection of deoxynivalenol (DON) using europium chelates and magnetic nanoparticles, Food Agric. Immunol. 30 (2019) 87–94, https://doi.org/10.1080/09540105.2018.1548577.